Structural size effect in capped metallic nanoparticles

Cora Moreira da Silva, Armelle Girard, Yann Le Bouar, Frédéric Fossard, Diana Dragoe, François Ducastelle, Annick Loiseau, Vincent Huc

Structural size effect in capped metallic nanoparticles

Cora Moreira Da Silva,[*,†] Armelle Girard,[†,‡] Yann Le Bouar,[†] Frédéric Fossard,[†] Diana Dragoe,[¶] François Ducastelle ,[a†] Annick Loiseau,[†] and Vincent Huc[¶]

†*Université Paris-Saclay, ONERA, CNRS, Laboratoire d'Étude des Microstructures, Châtillon, 92322, France*

‡*Université Paris-Saclay, UVSQ, 78000, Versailles, France*

¶*Université Paris-Saclay,CNRS, Institut de chimie moléculaire et des matériaux d'Orsay, 91405, Orsay, France*

E-mail:

coramoreiradasilva@gmail.com,vincent.huc@universite-paris-saclay.fr,annick.loiseau@onera.fr

Phone: +33 (0)1 46 73 45 63

[a]François Ducastelle was a physicist specialising in electronic structure of metals and their alloys, the statistical physics of order-disorder and phase transitions and the growth modes and spectroscopic properties of low-dimensional materials. He passed away on 2 July 2021.

Abstract

The surfactant used during a colloidal synthesis is known to control the size and shape of metallic nanoparticles. However, its influence on the nanoparticle (NP) structure is still not well understood. In this study, we show that the surfactant can significantly modify the lattice parameter of a crystalline particle. First, our electron diffraction measurements reveals that NiPt nanoparticles around 4 nm in diameter covered by a mixture of oleylamine and oleic acid (50:50) display a lattice parameter expansion around 2 % when compared to the same particles without surfactant. Using

high-resolution transmission electron microscopy (HRTEM), X-ray photoelectron spectroscopy (XPS) and energy-dispersive X-ray spectroscopy (EDX) techniques, we show that this expansion can not be explained by crystal defects, twinning, oxydation or atoms insertion. Then, using covered NPs in the 4 - 22 nm size range, we show that the lattice parameter evolves linearly with the inverse of the NP size, as it is expected when a surface stress is present. Finally, the study is extended to pure nickel and pure platinum NPs, with different sizes, coated by different surfactants (oleylamine, trioctylphosphine, polyvinylpyrrolidone). The surfactants induce lattice parameter variations, whose magnitude could be related to the charge transfert between the surfactant and the particle surface.

KEYWORDS: Lattice parameters, nanoparticle, surfactants, colloidal synthesis, transmission electron microscopy, surface stress

Metallic nanoparticles are now widely used, in various fields.[1–4] Their nanometric size gives them an important surface/volume ratio, allowing their use in catalysis (among others). These nanoobjects can be made in different ways, using the so-called physical route (ion sputtering, molecular beam epitaxy, pulsed laser deposition *etc.*) or chemical route (solution-phase processes, *etc.*). This paper focuses on NPs produced by the chemical route that requires few specific equipment and is usually easy to manage. This route is often based on the use of surfactants. These chemical species are amphiphilic compounds, with a chemical group ensuring compatibility with the solvent (generally made up of a long carbon chain) and an another one the adhesion to the NP surface. The bonding group can be of different types according to the NPs nature: cationic,[5,6] anionic,[7,8] amphoteric zwitterionic,[9,10] or nonionic.[11,12] They adsorb on NPs surface allowing for size and shape control and system stabilisation by bonds formation, reducing their surface energy (protection against ripening and oxidation). Surfactants can bind to particular atomic sites, with different affinities depending on the nanocrystal face to which they bind. It is also possible to control the nanocrystals

morphology by choosing surfactants that selectively bind to particular surfaces.[13–18]

A large number of publications deals with the influence of these molecules on NPs' morphology as well as on the catalytic,[19] magnetic,[20,21] *etc.* properties. However, information about their influence on the lattice parameter of NPs is still lacking. This information is clearly desirable because a variation of the lattice parameters can change the chemical and physical properties mentioned above. Most theoretical or experimental studies in the literature dealing with the lattice parameter of nanoparticles only consider particles without *chemical environment*[22]; A lattice parameter contraction is reported as metallic nanoobjects size decreases due to surface stress effect.[23–27] The few studies reporting lattice parameters measurements of covered nanoparticles use X-ray diffraction (XRD) powder analysis where particles are ground with a mortar, in air.[7,28] This can degrade and detach the surfactants so that this approach can not be used to accurately analyse the influence of surfactants on the lattice parameter. To avoid these phenomena, we use transmission electron microscopy (TEM) in diffraction and high resolution imaging mode to characterize the structure and in energy-dispersive X-ray spectroscopy (EDX) mapping mode to characterize the composition. The paper is organized as follows. In a first part, we consider nickel-platinum Ni-Pt alloy nanoparticles and we analyze, for different NPs sizes, the variation of the lattice parameter when the particle is covered by a mixture of oleylamine and oleic acid (50:50). In a second part, we use monometallic Ni or Pt nanoparticles to study how different types of surfactants with different bonding groups (oleylamine, trioctylphosphine and polyvinylpyrrolidone) modify the lattice parameters. Finally, we discuss the importance of the charge transfer between the surfactant and the particle.

Results

Size dependence of lattice parameters in capped NPs

In a previous work[29] we analyzed alloyed nanoparticles obtained by hot injection colloidal synthesis with a mixture of oleylamine (OAm) and oleic acid (OAc) as surfactants. The nanoobjects were studied by electron diffraction revealing an unexpected lattice parameter expansion, whatever NPs composition. To explain this expansion, four hypotheses were proposed: (*i*) presence of defects or crystal twinning into NPs, (*ii*) atoms incorporation into crystal lattice due to the *high* temperature synthesis, (*iii*) NPs oxidation or (*iv*) presence of organic molecules on NPs surface which induces a lattice parameter variation.

In the present work, we first present a comprehensive study to assess these different possibilities. Several analyses were carried out on the same solid solution alloy nanoparticles with $d = (4.1 \pm 0.7)$ nm in diameter. The composition of the particules, measured by EDX, is $Ni_{56}Pt_{44}$. For simplicity, we will refer to these nanoparticles as NiPt particles in the following. As in our previous work, we measure by electron diffraction a lattice parameter expansion $a = (0.373 \pm 0.003)$ nm which is significantly larger (about 2 %) than the lattice parameter of the corresponding bulk alloy, and thus larger than the expected lattice parameter of uncovered NPs. Before discussion the value of the lattice parameter, we present structural and chemical characterisations to assess the homogeneity of our particle. First, HRTEM analyses were performed on a large number of particles. Images in figure 1 show that all NPs have regular crystallographic planes, without defects or crystal twinning.

XPS analyses were then carried out on the same sample, in order to detect possible atoms insertion into the lattice. Figure 2 displays XPS signals obtained for each element composing the nanoparticle-surfactant system. The C_{15} core-level spectrum (Fig. 2, a.) shows peaks at 285 eV, 286.4 eV and 288.4 eV characteristic of C-C, C-O and COO bonds, confirming the presence of carbon atoms from the carbon chains of OAc and OAm and the OAc carboxyl function. It is important to note the absence of signals in the 280.5 - 283 eV energy window,

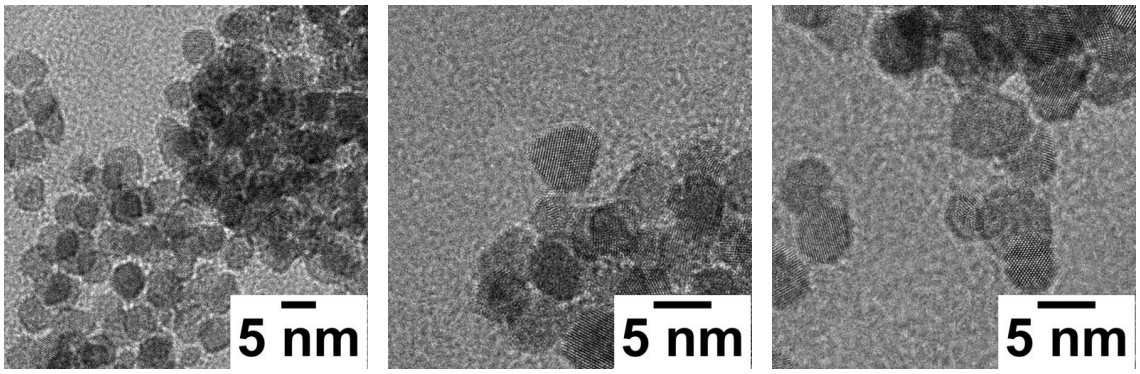

(a) (b) (c)

Figure 1: (a), (b), (c) HRTEM micrographies of solid solution NiPt nanoparticles.

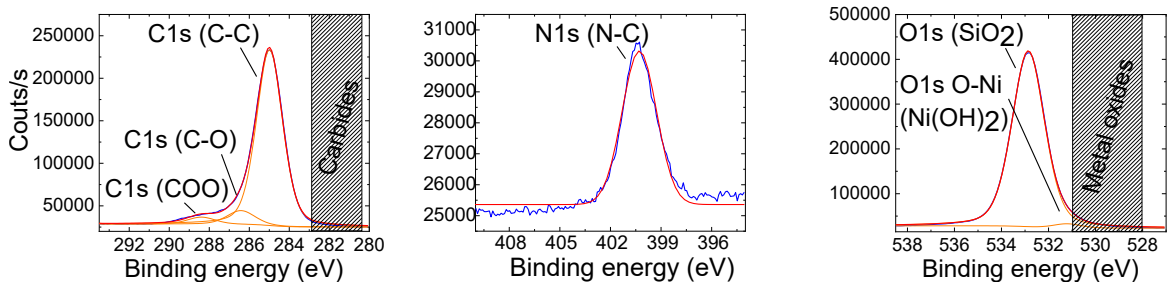

(a) (b) (c)

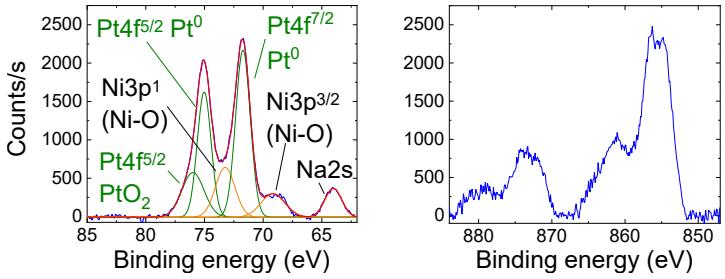

(d) (e)

Figure 2: XPS spectra of a drop of $Ni_{56}Pt_{46}$ colloidal solution deposited on SiO_2 wafer. With the signals of : (a) carbon, (b) nitrogen, (c) carbon, (d) platinum (in green) and nickel $3p$ (in orange) and (e) nickel $2p$. In blue : raw signal, in orange : deconvolution of the different peaks and in red : curve obtained by the sum of the deconvolutions of the different peaks. XPS survey in Fig. S1 of Supporting Information (SI) file.

characteristic of carbide compounds.[30] The hypothesis of the insertion of carbon atoms in the crystal lattice is thus ruled out. The figure 2, b. shows a peak at 400 eV, corresponding to N-C bond from the OAm surfactant. In figure 2, c. two peaks are observed. The first

one, very intense at 533 eV, feature of Si-O bonds, attribued to the substrate (silicon wafer coated with a 100 nm layer of silica). The second one, much lower, at 531.3 eV corresponds to the signal of Ni-OH bond, wich is explained by the bond between surface nickel and the OAc carboxyl function. The absence of metal oxide signal in the 528 - 531 eV[30] range is noted, but can also be explained by the predominance of the Si-O peak which can mask it. In figure 2, d. the two main peaks at 71.3 eV and 74.6 eV correspond to the signals of pure Pt, the shoulder observed at 75.6 eV can be attributed to Pt-O bonding signal (PtO_2).[30,31] Low intensity signals at 68.76 eV and 72.8 eV are attributed to Ni bound to O (Ni-O). The last one, at 63.6 eV, corresponds to Na2s. The shifts of Ni3p and Pt4$f^{5/2}$ signals (Fig. 2, d.) observed are due to the bonding between metal atoms and oxygen atoms present in the OAc carboxyl function. In figure 2, e., observed signal shows that nickel is on several forms: Ni^0, Ni-OH and Ni-O (as can be seen from the different signals compaison in Fig. S2 of SI), which is expected for a sample dried in air for XPS measurement.

To highlight the homogeneity of the NPs and the absence of an oxide layer on the NPs surface we chose EDX analyses in mapping mode coupled with high-angular dark field scanning TEM (STEM-HAADF). Using artificially oxidized transition metal NPs, we have verified that this technique is able to image an oxide layer around a particle (Fig. S3 of SI). Figure 3 compares oxygen (Fig. 3, b.) and nitrogen (Fig. 3, c.) signals. Oxygen signal has the same pattern as that of nitrogen, showing that oxygen is brought by the surfactant (OAc), as is nitrogen (OAm). It also and shows at the same time the absence of an oxide layer around NPs' surface.

From our structural and chemical analysis, we conclude that the particles do not contain crystalline defects and are homogeneous. The lattice parameter expansion is thus necessarily related to the organic molecules grafted on the NPs surface. This point can be confirmed by a simple heating experiment in a TEM. More precisely, the lattice parameters of particles surrounded by surface agents are monitored (by electronic diffraction) at different temperatures, until complete desorption/degradation of these organic molecules. Note that the

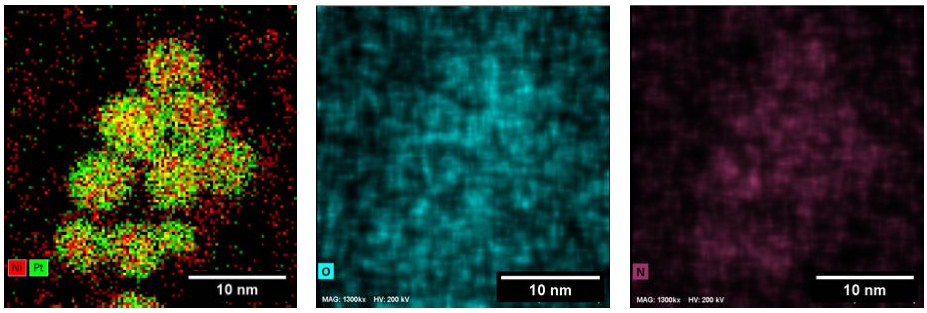

(a) (b) (c)

Figure 3: Transmission electron micrographs of alloyed NiPt NPs obtained in STEM-EDX mapping mode (a) with platinum (L_α line) in green and nickel (K_α line) in red signals (b) oxygen (K_α line) signal and (c) nitrogen (K_α line) signal.

boiling point of OAm and OAc are 364 °C and 360 °C, respectivly at atmospheric pressure. It can thus be safely assessed that at the working temperature and under UHV conditions, these surfactants will be completely removed from the surface. For this purpose, NPs are deposited on multi-walled carbon nanotubes (MWCNT). MWCNTs supports were used for a better thermal distribution over the whole TEM grid and to avoid graphitisation of the surfactants on the particles.[29] Once deposited, the NPs are heated up to 800 °C rapidly (~ 62 ° C/min) (a temperature flash allowing for a fast surfactants degradation) and rapidly cooled down to room temperature ($\sim$ 40 ° C/min until $\sim$ 40 ° C and $\sim$ 0.5 ° C/min to $\sim$ 23 ° C) before performing new electron diffractions, in order to avoid the contribution of thermal expansion on the lattice parameter value. Three regions are monitored : an extended zone containing a large and dense assembly of particles (Fig. 4, a.), a smaller and less dense assembly (Fig. 4, b.) and a third one containing only 5 particles (Fig. 4, c.).

For the large assembly, we observe after the heating procedure many coalesced particles, and the lattice parameter deduced from the electron diffraction is $a = (0.362 \pm 0.002)$ nm. For the smaller assembly, only a limited number of coalescence events can be seen and the measured lattice parameter is $a = (0.364 \pm 0.003)$ nm. For the 5 isolated NPs, we measure a lattice parameter $a = (0.363 \pm 0.005)$ nm. Thus, whatever the final appearance of the NPs after the heat treatment, we find a contraction of the order of 2.7 %. This result further

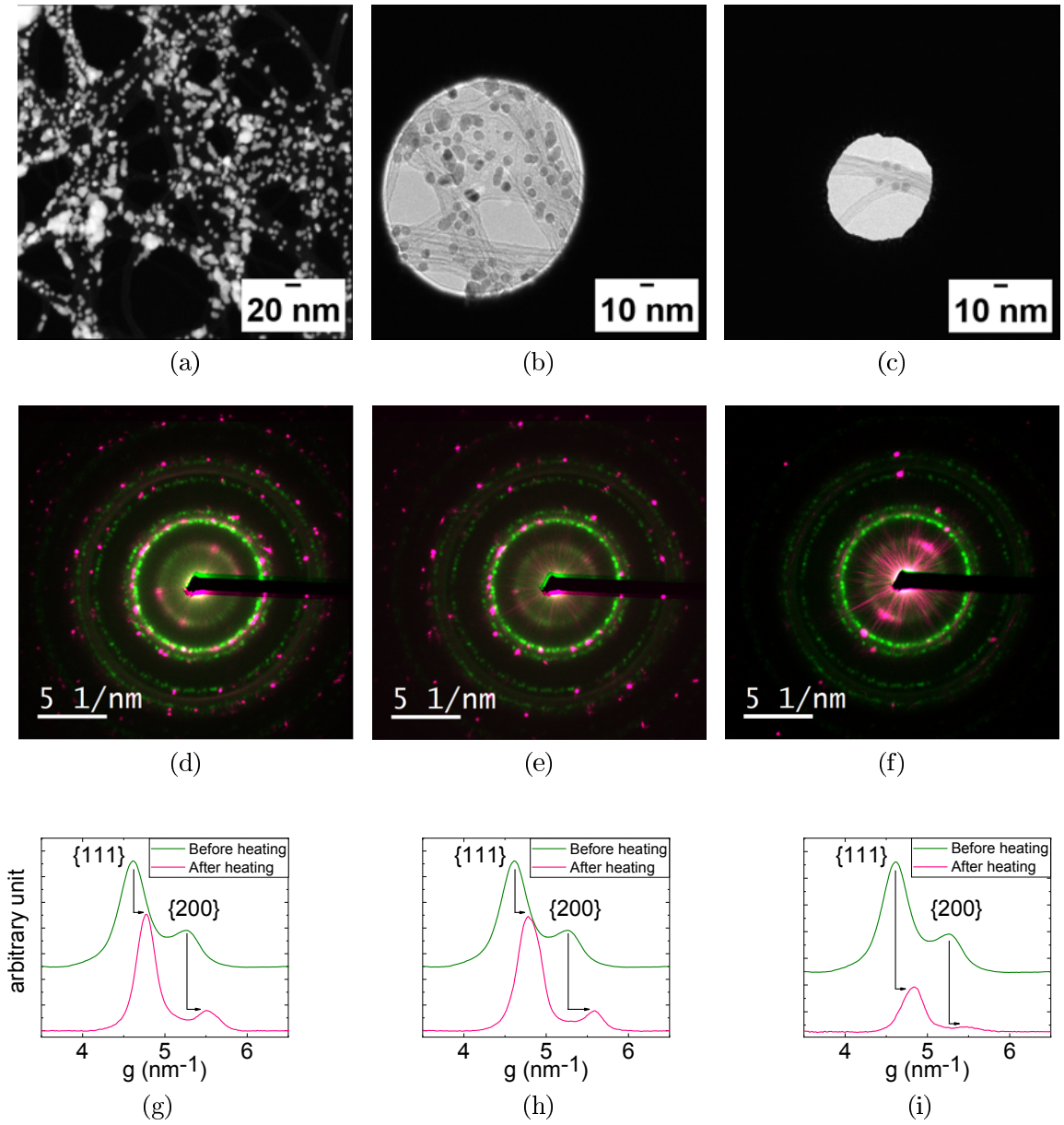

Figure 4: Electron micrographies of $Ni_{56}Pt_{44}$ after heating at 800 °C (a) 1^{st} area in HAADF-STEM mode, (b) 2^{nd} area with less coalesced particles and (c) 3^{rd} area of isolated NPs without coalescence.(d), (d) and (f) images are the superposition of the diffraction images at room temperature (green) and the diffraction images after heating (in pink) and the (g), (h), (i) rotational average in function of g (scattering vector) of the (d), (e) and (f) zones respectively.

evidences that the presence and/or absence of surfactants has a significant influence on the lattice parameter of the NPs. Because the organic molecules are attached to the NP surface, we expect that their influence will scale with the surface area. As it is well known in the

context of NPs, the competition between surface and bulk effects leads to size dependance. In particular, the surface stress is known to induce a lattice parameter variation inversely proportional to the NPs diameter. With this in mind, four samples of Ni-Pt NPs (with a composition close to equimolarity), with different sizes (4.1 nm, 4.7 nm, 7 nm, 22 nm), were synthesized and observed by TEM (bright field and electron diffraction mode). The measures, presented in Fig. 5, reveal a linear correlation between the relative variation of the lattice parameter and the inverse of the NPs' size. This size effect can be explained within a simple mechanical model which includes the elastic behavior of interfaces. Because atoms close to the surface differ in local environment from the atom in the bulk material, even when there is no stress in the bulk (*i.e.* the lattice parameter is the equilibrium lattice parameter a_{bulk} of the bulk), it remains a surface stress.[32] More precisely, the surface stress is, like the surface energy, an excess quantity and is expressed in N/m. Based on this concept, the evolution of the lattice parameter as a function of its size can be explained using a simple isotropic mechanical model for a spherical NP.[33,34] The equilibrium lattice parameter a of a NP is related to its diameter D by:

$$\frac{a - a_{bulk}}{a_{bulk}} = \frac{-4f}{3B} \cdot \frac{1}{D} \tag{1}$$

where f is the surface stress and B the bulk modulus. If we assume that the influence of the surfactant is limited to a modification of the surface of the NP, this model predicts a linear relationship between the lattice parameter and the inverse of the NP size. The results presented in Fig. 5 are consistent with this behavior. Indeed, even if the line does not exactly go through 0, this can be explained by a small error on lattice parameters deduced from electron diffraction patterns (~ 0.0018 nm), or a small error on the value used for the bulk compound.

The slope of the line in Fig. 5 can then be interpreted as an effective surface stress (for

the surface with surfactants) equal to $f_{eff} = -29$ N/m (the value of the bulk modulus $B_{NiPt} = 234.5$ GPa is obtained by interpolating the values of B_{Ni},[35] B_{Pt},[35] B_{Ni_3Pt},[36] B_{NiPt_3}[37] at 300 K). In absolute value, this value is one order of magnitude higher than the surface stress of free surfaces.[32] But, more important than the value of f_{eff}, is its sign. This negative stress implies a tensile force on the NP, in line with the observed lattice parameter expansion. This result is surprising because, for metallic NPs, the many body character of the metal bonding is known to cause positive surface stress and thus a contraction of the lattice parameter.[32]

Note that the mechanical model presented above is based on a continuous formalism and therefore does not require an atomic description of the interface: only the elastic behavior of the interface is of importance. The model also assumes that the mechanical equilibrium is always reached, an assumption that is clearly fulfilled at the time scale of the experiment.[38] Finally, we stress that the model shows that the lattice parameter is homogeneous *within the NP*, but its application to the description of the outer interplane distance could be questionable due to the continuous character of the approach. The model is thus unable to describe the anisotropic and inhomogeneous strains that may appear at the NP surface, which can be related to the coordination-number/bond-length at the surface or to geometrical effects.[22] These local strains have been recently revealed using experimental techniques such as Peak Finding (PF)[49] or Geometric Phase Analysis (GPA)[50] which are digital signal processing techniques enabling local measurements of atomic displacements. However, these techniques are difficult to apply to small particles surrounded by an organic layer because this layer causes electron diffusion (HRTEM) or electron-beam-induced carbon contamination (STEM)[51] phenomenon, that affect the quality of the images. How the presence of a surfactant modifies these local strains is out of the scope of the present paper, which is focused on the average strain in the NP.

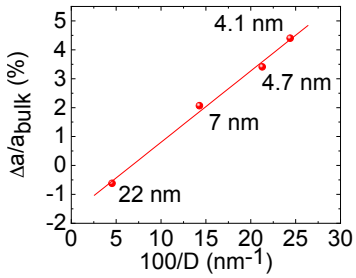

Figure 5: Relative variation of the lattice parameter $(a - a_{bulk})/a_{bulk}$ (%) as a function of the inverse diameter (100/D) of NiPt NPs. The bulk lattice parameter is $a_{bulk,NiPt} = 0.3750$ nm.[39]

Influence of surfactants' nature on nanoparticles

To further understand the surfactants influence on NPs lattice parameters, monometallic NPs (in which surface segregation can not occur[22]) were then studied. Three different linear and monodentate surfactants widely used in solution synthesis are considered: oleylamine (OAm), trioctylphosphine (TOP) and polyvinylpyrrolidone (PVP) (Fig. 6).

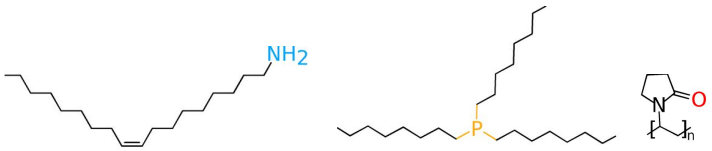

(a) (b) (c)

Figure 6: Chemical structure of (a) oleylamine $C_{18}H_{35}NH_2$, (b) trioctylphospine $C_{24}H_{51}P$ and (c) polyvinylpyrrolidone $(C_6H_9NO)_n$ with their particule attachment group coloured.

First, various monometallic nickel NPs, with different sizes are synthesized, using two surfactants : OAm and TOP (see Fig. S4 and S5 of SI). PVP has not been used here because this surfactant is used in aqueous media, where nickel NPs are likely to be oxidized, rendering them unusable for this study. As previously, the relative variation of the lattice parameter $\Delta a/a_{bulk}$ (%) is plotted versus $100/D$ (see Fig. 7).

Figure 7, a. shows a linear correlation between $\Delta a/a_{bulk}$ and $1/D$ for Ni-OAm particles. Here, the value $f_{eff} = -68$ N.m^{-1} can be deduced from the slope. It is observed, at small sizes $\sim$ 2.5 nm, a lattice parameter expansion around 20 %. Because this value is huge,

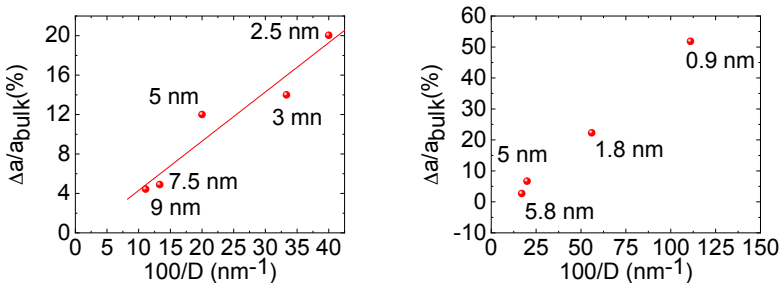

(a) (b)

Figure 7: Relative variation of the lattice parameter $\Delta a/a_{bulk}$ (%) as a function of 100/D of (a) Ni-OAm NPs and (b) Ni-TOP NPs.

HRTEM analyses were carried out to investigate if the NPs remain crystalline and homogeneous. Even if the presence of the surfactants impacts the images, we were able to conclude that all the observed NPs are consistent with a homogeneous defect-free FCC structure: no dislocation, planar defects or crystal twinning could be observed (Fig. 8, a.). Note that, due to the presence of the surfactant, our HRTEM images are not able to reveal an eventual reconstruction of the NP surface. The NPs *in situ* monitoring by electron diffraction (according to the same protocol used above for $Ni_{56}Pt_{44}$ particles) during surfactant degradation shows that the NP remains FCC and that the lattice parameter decreases. This contraction is nearly 18 %, so that the lattice parameter reaches value close to the bulk nickel lattice parameter (Fig. 8, b.). It can thus be concluded that the observed expansion of the lattice prameter is, also here, directly related to the presence of organic species on the NPs' surface.

A similar increase of the lattice parameter when decreasing the NP size is observed for Ni-TOP system (Fig. 7, b). However, HRTEM images show that these particles are crystalline but contain defects (stacking defects, twin planes, ...), especially for small sizes (Fig. 9). This shows a strong influence of TOP on the structure of the nickel NPs, but the description of an homogeneous NP with a surface modified by the surfactant used in Eq. 1 cannot be applied here.

The same study was then realized using platinum particles with OAm, TOP and PVP as

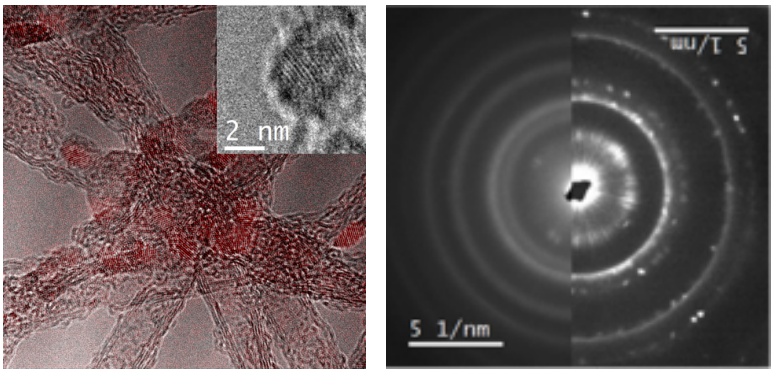

(a) (b)

Figure 8: (a) HRTEM image of Ni-OAm NPs (highlighted in red) deposited on MWCNTs before heating treatment, showing regular crystal planes without deformation (in inset) and (b) at the left : electron diffraction pattern before heating at 800 °C corresponding to a lattice parameter $a = (0.428 \pm 0.003)$ nm. Note that diffuse lines are observed. This effect is due to the low ratio of metal atoms *vs.* surfactants (see SI for details). At the right : the same area after heating. The measured lattice parameter ($a = (0.362 \pm 0.003)$ nm) has significantly decreased and is still above bulk value, but nickel is known to solubilize carbon atoms at high temperatures,[40] which may explain this residual expansion. Note that the diffraction lines are less diffuse, due to the removal of organic matter.

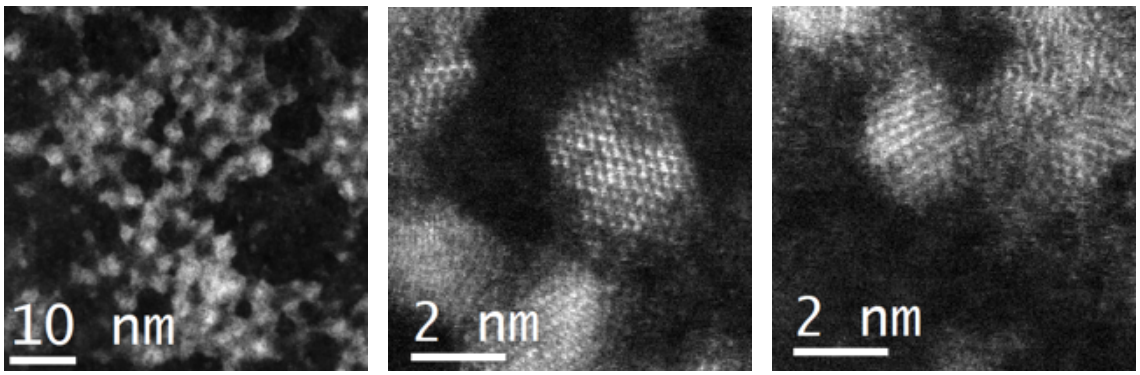

(a) (b) (c)

Figure 9: (a) HR-STEM images of Ni-TOP NPs and (b),(c) zoom on isolated NPs showing stacking defects.

surfactants. We have verified that, for all sizes, the NPs are monodisperse and crystalline (see Fig. S6, S7, S8 of SI). Figure 10 gathers the measurements of the lattice parameters for all the Pt particles. As for the nickel particles, all measurements are consistent with linear correlations between $\Delta a/a_{bulk}$ and $1/D$. However, the observed lattice parameter variations are smaller and do not exceed 4 %. In the cases of Pt-OAm and Pt-TOP, the slopes are of

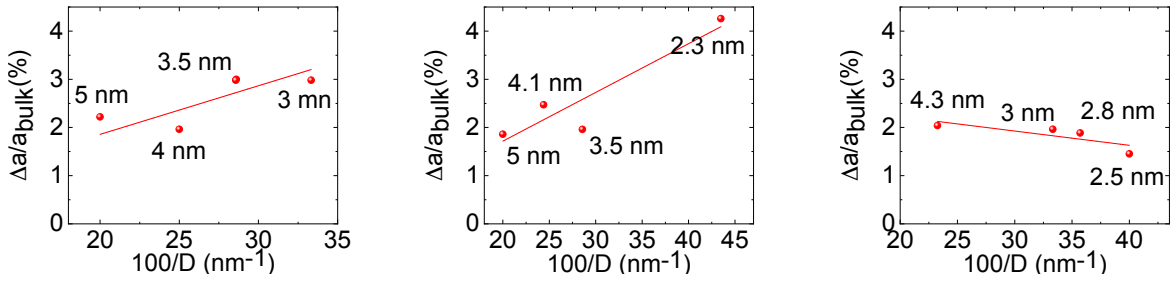

(a) (b) (c)

Figure 10: Relative variation of the lattice parameter $\Delta a/a_{bulk}$ (%) as a function of the diameter (100/D) of (a) Pt-OAm NPs, (b) Pt-TOP NPs and (c) Pt-PVP NPs.

same sign as those of Ni-OAm and Ni-TOP, implying a negative effective surface stress. On the contrary, for Pt-PVP (Fig. 10, c.), the surface stress f_{eff} is positive, *i.e.* of the same sign as for a free surface. All the effective surface stresses obtained for capped Ni and Pt particles are gathered in Table 1.

Table 1: Summary table of effective surface stresses obtained in Fig. 7 and 10

System	f_{eff} (N.m^{-1})
Ni-OAm	- 68
Pt-OAm	- 18
Pt-TOP	- 20
Pt-PVP	+ 6

Discussion

It was shown, in both pure and alloy NPs, that the lattice parameter varies approximately linearly with the inverse of the NPs size and that the slope depends on the surfactant present on the surface of the particles. In almost all considered cases, the NPs are crystalline and no defect or inhomogeneity could be observed. Therefore, the lattice parameter variation could be explained by a simple isotropic mechanical model, in which the elastic behavior of the interface is dependant on the surfactant. However, when compared to the case of uncapped

NPs, the measured surface stress can be one order of magnitude higher, and with a different sign. In this part, we discuss the origin of the surface stress in capped particles and how its value is related to the choice of the surfactant. Several experimental reports, including *in situ* TEM observations, show that the lattice parameter depends significantly on environmental conditions.[27,41–46] Diehm *et al.* have detailed the possible origins of lattice parameter variations. For purely metallic materials, a lattice parameter contraction is observed (positive surface stress) due to the resistance of metallic bonds which increases continuously with the decreasing number of coordination.[27] In most cases, as a bond strength increases, its length decreases.[47] The less coordinated surface atoms are in tensile state, which increases the reactivity of the surface and makes the NPs prone to chemical reactions and/or coalescence events. In the presence of surfactants, sub-coordinated surface atoms bind with this organic molecules to gain in stability. This new bond between the surfactant and the surface makes the surface atoms an inorganic complex-like specie, becoming more pronounced with decreasing NPs size, due to the increasing predominance of surface over volume. Dassenoy *et al.*[48] and Chakroune *et al.*[20] demonstrated this phenomenon by comparing NPs with different sizes of Pt coated by polymers *vs.* octanethiol as surfactants and Ru coated by acetate *vs.* dodecanethiol. They observed that, in the case of particles coated by thiol surfactants (which contain a highly coordinating sulphur atom), the formation of strong bonds between the surfactant and the NP surface atoms leads to a NPs structure with a well crystallized core and a disorganized outer layer, in contrast to particles coated with other surfactants. They attribute this difference in behaviour to the very high charge transfer in the case of thiols *via* the sulphur atom, including the creation of sulphide compounds at NPs surfaces. The very strong influence of TOP as a surfactant on the NP structure was also observed in our work. Indeed, HRTEM images have revealed that Ni-TOP particles contains crystalline defects (Fig. 9), unlike NPs coated by OAm/OAc (Fig. 1) and OAm (Fig. 8). Several experimental and theoretical studies have demonstrated that the absorption of absorbates on surface can lead to distortions of the outermost one, or more layers or even reconstruction of

the surface, by electronic structure effects.[52–54] Ibach *et al.* showed that the charge transfer direction of absorbates-surface atoms bonds controls the sign of the surface stress.[55] For OAm and TOP surfactants, anchor atoms are nitrogen and phosphorus, both are σ donors due to their free electron doublet,[56] and we observe that both generate negative values of f_{eff}. PVP is physisorbed on NPs surface,[57–59] only Van der Waals interactions are involved, so there is no charge transfert, which is consistent with the small and positive values of f_{eff} (see Tab. 1), which are close to that found for nanoparticles without a chemical environment.[23–26] The charge transfer derives from electron coupling between d orbitals of metal and ligands energy levels. The strength of this interaction depends on the relative position of HOMO and LUMO orbitals of the ligand, with respect to the metal Fermi level and can be interpreted invoking the Hard-Soft Acid-Base (HSAB) theory.[19] According to this theory, a hard acid reacts preferentially with a hard base; similarly for a soft acid with a soft base. The most stable interactions of acids and bases are hard-hard (ionic character) and soft-soft (covalent character). If we refer to the Fig. 11, platinum (soft acid) establishes more stable

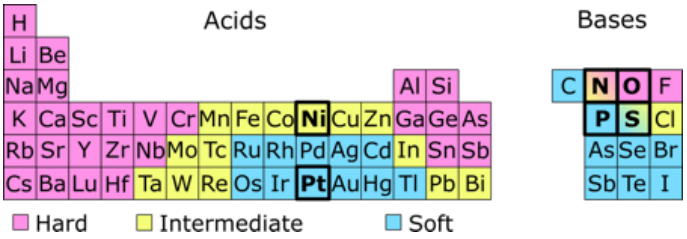

Figure 11: Periodic table with coloring according with HSAB theory.

bonds with atoms in following order: P (TOP) > N (OAm), which is in agreement with the absolute values obtained in Tab. 1. For nickel (intermediate acid), the deduced stability order is : N (OAm) > P (TOP). The strong bonds predicted for Ni with OAm are consistent with the large value of the surface stress reported in Tab. 1. Concerning the Ni-TOP particles, the existence of crystalline defects could be explained by the π acceptor character of P (in addition to its σ donor character), which also contributes to a higher bond strength compared to that with OAm.[56]

Note that, despite the use of identical surfactants (OAm and TOP), the absolute values of f_{eff} are higher for Ni than for Pt. A full explanation of this phenomenon requires electronic structure calculations of Ni and Pt surfaces in the presence of surfactants.

Conclusions

Differents NPs (NiPt, Ni and Pt), obtained by colloidal synthesis, have shown lattice parameter variations depending on their size and their chemical environment (OAm+OAc, OAm, TOP and PVP). After eliminating possible effects associated with the presence of defects (HRTEM), atoms insertion (XPS, EDX) or NPs oxidation (EDX), *in situ* monitoring of electron diffraction during particle heating (inducing surfactant degradation) has shown a convergence of the lattice parameters to expected values. This is a strong evidence that the observed lattice parameter variation is due to the presence of surface agents on NPs. Finally, the use of mechanical elastic model have demonstrated an linear variation of lattice parameter with NPs diameter, confirming that this variation is due to a surface phenomenon. The sign and the value of the surface stress extracted from the model depends on the nature of the attachment part of the organic molecule and the chemical element component the NPs. Given the latest theoretical and experimental works showing the strains inhomogeneous character and the knowledge that surfactants can bind to particular crystallographic sites, more local strains analyses are needed but are still challenging due to the presence of long organic chains on NPs surface. In addition, several phenomena must come into play during the formation of the bond and in the ensuing phenomena, requiring further studies on the subject. The conclusion of this work is that the use of surfactant during synthesis is not as trivial as it may appear at first sight. The surfaces of nanoparticles are interfaces, with a multitude of phenomena acting at the same time and that what happens at this interface can influence the whole particle.

Methods

Experimental Procedure

Nanoparticles synthesis

To prevent contaminations, all laboratory glasswares were washed by *aqua regia* (nitric acide 1 : 3 hydrochloric acid) during (at least) five hours and rinsed with large amounts of distilled water, dichloromethane (DCM) and acetone. Synthesis were carried out under argon blanket. Commercial reagents were used without purification.

Ni-OAm / Pt-OAm Typically, to obtain *spherical type* nanoparticles with 4 - 5 nm in diameter, 3 mL of oleylamine (OAm) (Acros Organics, 80 - 90 %) used as surfactant and solvent also, 0.0254 mmol of precursor ($Pt(acac)_2$ (Aldrich, 99 %) or $Ni(acac)_2$ (Aldrich, 95 %)) and 0.124 mmol tetra-*n*-butylammonium bromide (TBAB) (TCI, 95 %) were added to a 100 mL round-bottom flask with a PTFE coated magnetic stir bar. The mixture was purged by 3 vacuum/argon cycles and heated during 10 min at 100 °C under vigorous stirring, to remove any water trace and prevent particle oxidation.
After the 10 min, the temperature was quickly raised until the solution turns black, proof of the NPs nucleation. The suspension was kept at the nucleation temperature during 10 min before being cooled down to room temperature under argon blanket. The suspension was purified by adding 20 mL of ethanol (EtOH) and was centrifuged at 10000 rpm for 20 min. The supernatant was separated and the precipitate was washed again with EtOH and centrifuged. The precipitate was redispersed in 30 mL of DCM.
To obtain NPs of different sizes, the parameters to be varied are: the quantity of reducing agents and the reaction time.

Ni-TOP / Pt-TOP The same procedure descrived for Ni-OAm and Pt-OAm are repeated by replacing OAm by TOP (AcroSeal, Thermo Scientific, 90 %) as surfactant and solvent.

Pt-PVP To obtain Pt-PVP particles, in reflux assembly, 100 mg of PVP (Mw $\sim$ 3500), 11.3 mL of methanol, 1 mL of distilled water and 0.31 mL of $H_2.PtCl_6$ were added to a 100 mL round-bottom flask with a PTFE coated magnetic stir bar. The mixture was heated to reflux under vigorous stirring. To obtain particles with different sizes, samples were collected (using a syringe) at different reaction times: 20 min, 25 min, 40 min, 60 min after the solution has turned black (proof of nucleation).

NPs characterizations

TEM analyses

As-synthesized NPs were characterized using Transmission Electron Microscopy (TEM). A drop of colloidal suspension was deposited and dried on copper TEM grid. The TEM grid was then gently rinsed with EtOH, using a Büchner filtration set-up. Size distribution (on population of 500 particles in 5 distinct zones on TEM grid and counted with Image J software) and electron diffraction were measured using a FEI-CM 20 TEM (200 kV). High-Resolution Transmission Electron Microscopy (HRTEM), High-Angle Annular Dark-Field imaging (STEM-HAADF) and electron diffraction were operated on a ZEISS-LIBRA 200 MC TEM. To support the results, UHRSTEM and chemical mapping were performed using a Titan G2 Cs-corrected FEI TEM operating at 200 kV on individual particles.

XPS analyses

X-ray photoelectron spectroscopy (XPS) measurements were performed on a Thermo Fischer Scientific instrument with a monochromatic Al-K_α X-ray source (energy 1486.7 eV). The base pressure was around $5*10^{-9}$ mbar and the diameter of the X-ray beam spot was 400 μm, corresponding to an irradiated surface of approximately 0.5 mm^2. The hemispherical analyzer was operated at 0 °take-off angle in the Constant Analyzer Energy (CAE) mode. Wide scan spectra were recorded at pass energy of 200 eV and an energy step of 1 eV while narrow

scan spectra were recorded at pass energies of 100 eV and 50 eV with an energy step of 0.1 eV. Charge compensation was achieved with the help of a "dual beam" flood gun using low-energy electrons ($\leq$ 5 eV) and argon ions. The binding energy scale was calibrated on the neutral carbon set at 285 eV.

Temperature experiments

To observe lattice parameter variation, with the surfactants thermal degradation, E GATAN heating sample holder on the ZEISS-LIBRA 200 MC TEM was used.

First, to deposite the NPs and guarantee a good thermal diffusion on the grid, a drop of multi-walled carbon nanotubes (ultrasound dispersed on DCM) was deposited and dried on NiC holey TEM grid. After, the grid was rinsed with low isopropanol flow to remove the excess of MWCNTs and other impurities. When the grid was dried, a drop of NPs-contained suspension was deposited and dried, and was rinsed with isopropanol once again to ensure a clean sample, free of particle build-up.

After selecting a working zone, where the NPs are numerous but far enough away for prevent ripening phenomena induced by temperature, a bright-field TEM and diffraction electron images were required and were repeted at several temperature.

Acknowledgement

The authors thank ANR GiANT (N °ANR-18-CE09-0014-04) and ARF "Nano" of ONERA for the financing of this work. HRSTEM-EDX study was carried out within the MATMECA consortium, supported by the ANR-10-EQPX-37 contract and has benefited from the facilities of the Laboratory MSSMat (now LMPS), CentraleSupélec. C.MDS would like to warmly thanks Ileana Florea for the method of depositing nanoparticles on MWCNTs and Souad Ammar-Merah, Nguyet-Thanh Ha-Duong and Sendos Darwich for the fruitful discussions.

Supporting Information Available

Additional XPS analyses and TEM observations (images and electron diffractions for each sample studied in this article) are presented and detailed in Supporting Information file.

References

(1) Jürgens, B.; Borchert, H.; Ahrenstorf, K.; Sonström, P.; Pretorius, A.; Schowalter, M.; Gries, K.; Zielasek, V.; Rosenauer, A.; Weller, H.; Bäumer, M. Colloidally prepared nanoparticles for the synthesis of structurally well-defined and highly active heterogeneous catalysts. Angewandte Chemie - International Edition **2008**, 47, 8946–8949.

(2) McEnaney, J. M.; Soucy, T. L.; Hodges, J. M.; Callejas, J. F.; Mondschein, J. S.; Schaak, R. E. Colloidally-synthesized cobalt molybdenum nanoparticles as active and stable electrocatalysts for the hydrogen evolution reaction under alkaline conditions. J. Mater. Chem. A **2016**, 4, 3077–3081.

(3) Kim, S.-W.; Son, S. U.; Lee, S. S.; Hyeon, T.; Chung, Y. K. Colloidal cobalt nanoparticles: a highly active and reusable Pauson–Khand catalyst. Chem. Commun. **2001**, 2212–2213.

(4) Schütte, K.; Doddi, A.; Kroll, C.; Meyer, H.; Wiktor, C.; Gemel, C.; van Tendeloo, G.; Fischer, R. A.; Janiak, C. Colloidal nickel/gallium nanoalloys obtained from organometallic precursors in conventional organic solvents and in ionic liquids: noble-metal-free alkyne semihydrogenation catalysts. Nanoscale **2014**, 6, 5532–5544.

(5) Chen, M.; Nikles, D. E. Synthesis, Self-Assembly, and Magnetic Properties of FexCoyPt100-x-y Nanoparticles. Nano Letters **2002**, 2, 211–214.

(6) Brinzei, D.; Catala, L.; Rogez, G.; Gloter, A.; Mallah, T. Magnetic behaviour of neg-

atively charged nickel(II) hexacyanoferrate(III) coordination nanoparticles. Inorganica Chimica Acta **2008**, 361, 3931–3936.

(7) Carenco, S.; Boissière, C.; Nicole, L.; Sanchez, C.; Floch, P. L.; Mézailles, N. Controlled design of Size-tunable monodisperse nickel nanoparticles. Chemistry of Materials **2010**, 22, 1340–1349.

(8) Chen, S.; Kimura, K. Synthesis of thiolate-stabilized platinum nanoparticles in protolytic solvents as isolable colloids. Journal of Physical Chemistry B **2001**, 105, 5397–5403.

(9) Salkar, R. A.; Jeevanandam, P.; Kataby, G.; Aruna, S. T.; Koltypin, Y.; Palchik, O.; Gedanken, A. Elongated Copper Nanoparticles Coated with a Zwitterionic Surfactant. Journal of Physical Chemistry B **2000**, 104, 893–897.

(10) Pallavicini, P.; Chirico, G.; Collini, M.; Dacarro, G.; Donà, A.; D'Alfonso, L.; Falqui, A.; Diaz-Fernandez, Y.; Freddi, S.; Garofalo, B.; Genovese, A.; Sironi, L.; Taglietti, A. Synthesis of branched Au nanoparticles with tunable near-infrared LSPR using a zwitterionic surfactant. Chemical Communications **2011**, 47, 1315–1317.

(11) Osseo-Asare, K.; Arriagada, F. J. Preparation of SiO2 nanoparticles in a non-ionic reverse micellar system. Colloids and Surfaces **1990**, 50, 321–339.

(12) Lee, J. H.; Park, B. E.; Lee, Y. M.; Hwang, S. H.; Ko, W. B. Synthesis of fullerene[C60]-silver nanoparticles using various non-ionic surfactants under microwave irradiation. Current Applied Physics **2009**, 9, 152–156.

(13) Peng, X.; Manna, L.; Yang, W.; Wickham, J. Shape Control of CdSe Nanocrystals Shape control of CdSe nanocrystals. Nature **2000**, 404, 59–61.

(14) Peng, Z.; Yang, H. Designer platinum nanoparticles: Control of shape, composition in alloy, nanostructure and electrocatalytic property. Nano Today **2009**, 4, 143–164.

(15) Bratlie, K. M.; Lee, H.; Komvopoulos, K.; Yang, P.; Somorjai, G. A. Platinum nanoparticle shape effects on benzene hydrogenation selectivity. Nano Letters **2007**, 7, 3097–3101.

(16) Ren, J.; Tilley, R. D. Shape-controlled growth of platinum nanoparticles. Small **2007**, 3, 1508–1512.

(17) Qu, L.; Dai, L.; Osawa, E. Shape/size-controlled syntheses of metal nanoparticles for site-selective modification of carbon nanotubes. Journal of the American Chemical Society **2006**, 128, 5523–5532.

(18) Song, H.; Kim, F.; Connor, S.; Somorjai, G. A.; Yang, P. Pt nanocrystals: Shape control and Langmuir-Blodgett monolayer formation. Journal of Physical Chemistry B **2005**, 109, 188–193.

(19) Campisi, S.; Schiavoni, M.; Chan-Thaw, C.; Villa, A. Untangling the Role of the Capping Agent in Nanocatalysis: Recent Advances and Perspectives. Catalysts **2016**, 6, 185.

(20) Chakroune, N.; Viau, G.; Ammar, S.; Poul, L.; Veautier, D.; Chehimi, M. M.; Mangeney, C.; Villain, F.; Fiévet, F. Acetate- and thiol-capped monodisperse ruthenium nanoparticles: XPS, XAS, and HRTEM studies. Langmuir **2005**, 21, 6788–6796.

(21) Abdolrahimi, M.; Vasilakaki, M.; Slimani, S.; Ntallis, N.; Varvaro, G.; Laureti, S.; Meneghini, C.; Trohidou, K. N.; Fiorani, D.; Peddis, D. Magnetism of nanoparticles: Effect of the organic coating. Nanomaterials **2021**, 11, 1787 (16).

(22) Nelli, D.; Roncaglia, C.; Minnai, C. Strain engineering in alloy nanoparticles. Advances in Physics: X **2023**, 8, 2127330.

(23) Yao, Y.; Wei, Y.; Chen, S. Size effect of the surface energy density of nanoparticles. Surface Science **2015**, 636, 19–24.

(24) Qi, W. H.; Wang, M. P. Size and shape dependent lattice parameters of metallic nanoparticles. Journal of Nanoparticle Research **2005**, 7, 51–57.

(25) Lamber, R.; Wetjen, S.; Jaeger, N. I. Size dependence of the lattice parameter of small palladium particles. Physical Review B **1995**, 51, 10968–10971.

(26) Huang, Z.; Thomson, P.; Di, S. Lattice contractions of a nanoparticle due to the surface tension: A model of elasticity. Journal of Physics and Chemistry of Solids **2007**, 68, 530–535.

(27) Diehm, P. M.; Ágoston, P.; Albe, K. Size-dependent lattice expansion in nanoparticles: Reality or anomaly? ChemPhysChem **2012**, 13, 2443–2454.

(28) Ahrenstorf, K.; Albrecht, O.; Heller, H.; Kornowski, A.; Görlitz, D.; Weller, H. Colloidal synthesis of NixPt1-x nanoparticles with tuneable composition and size. Small **2007**, 3, 271–274.

(29) Moreira Da Silva, C.; Girard, A.; Dufond, M.; Fossard, F.; Andrieux-Ledier, A.; Huc, V.; Loiseau, A. Nickel platinum (NixPt1x) nanoalloy monodisperse particles without the core shell structure by colloidal synthesis. Nanoscale Advances **2020**, 2, 3882–3889.

(30) Moulder, J. F.; Stickle, W. F.; Sobol, P. E.; Bomben, K. D. In Handbook of X-ray Photoelectron Spectroscopy; Chastain, J., Ed.; Perkin-Elmer Corporation - Physical Electronics Division, 1992.

(31) Ono, L. K.; Yuan, B.; Heinrich, H.; Cuenya, B. R. Formation and thermal stability of platinum oxides on size-selected platinum nanoparticles: support effects. The Journal of Physical Chemistry C **2010**, 114, 22119–22133.

(32) Müller, P.; Saúl, A. Elastic effects on surface physics. Surface Science Reports **2004**, 54, 157–258.

(33) Mays, C. W.; Vermaak, J. S.; Kuhlmann-Wilsdorf, D. On surface stress and surface tension. II. Determination of the surface stress of gold. Surface Science **1968**, 12, 134–140.

(34) Le Bouar, Y. In Mechanics of nano-objects; O. Thomas, S. F., A. Ponchet, Ed.; Les Presses de l'École des Mines de Paris, 2011; Chapter An introduction to the stability of nanoparticles, pp 213–240.

(35) Cagin, T.; Dereli, G.; Uludogan, M.; Tomak, M. Thermal and mechanical properties of some fcc transition metals T. Physical Review B **1999**, 59, 3468 – 3473.

(36) Chen, Q.; Huang, Z.; Zhao, Z.; Hu, C. First-principles study on the structural, elastic, and thermodynamics properties of Ni3X (X: Al, Mo, Ti, Pt, Si, Nb, V, and Zr) intermetallic compounds. Applied Physics A: Materials Science and Processing **2014**, 116, 1161–1172.

(37) Rajagopalan, M. Full potential linear augmented plane wave study of the elastic properties of XPt3 (X=V, Cr, Mn, Fe, Co, Ni). Physica B: Condensed Matter **2010**, 405, 2516–2518.

(38) Kittel, C.; McEuen, P. Introduction to solid state physics; John Wiley & Sons, 2018.

(39) Villars, P. In Pearson's Handbook: Desk Edition: Crystallographic Data for Intermetallic Phases; International, A., Ed.; 1997.

(40) Diarra, M.; Amara, H.; Ducastelle, F.; Bichara, C. Carbon solubility in nickel nanoparticles: A grand canonical Monte Carlo study. Physica Status Solidi (B) Basic Research **2012**, 249, 2629–2634.

(41) Hansen, P. L.; Wagner, J. B.; Helveg, S.; Rostrup-Nielsen, J. R.; Clausen, B. S.; Topsøe, H. Atom-Resolved Imaging of Dynamic Shape Changes in Supported Copper Nanocrystals. Science **2002**, 295, 2053–2055.

(42) Yoshida, H.; Kuwauchi, Y.; Jinschek, J. R.; Sun, K.; Tanaka, S.; Kohyama, M.; Shimada, S.; Haruta, M.; Takeda, S. Visualizing gas molecules interacting with supported nanoparticulate catalysts at reaction conditions. Science **2012**, 335, 317–319.

(43) Kuwauchi, Y.; Yoshida, H.; Akita, T.; Haruta, M.; Takeda, S. Intrinsic catalytic structure of gold nanoparticles supported on TiO 2. Angewandte Chemie - International Edition **2012**, 51, 7729–7733.

(44) Zhang, S.; Plessow, P. N.; Willis, J. J.; Dai, S.; Xu, M.; Graham, G. W.; Cargnello, M.; Abild-Pedersen, F.; Pan, X. Dynamical observation and detailed description of catalysts under strong metal-support interaction. Nano Letters **2016**, 16, 4528–4534.

(45) Nian, Y.; Dong, Z.; Wang, S.; Wang, Y.; Han, Y.; Wang, C.; Luo, L. Atomic-Scale Dynamic Interaction of H2 O Molecules with Cu Surface. Physical Review Letters **2020**, 125, 15101 (5).

(46) Luo, L.; Chen, S.; Xu, Q.; He, Y.; Dong, Z.; Zhang, L.; Zhu, J.; Du, Y.; Yang, B.; Wang, C. Dynamic Atom Clusters on AuCu Nanoparticle Surface during CO Oxidation. Journal of the American Chemical Society **2020**, 142, 4022–4027.

(47) Zhao, L.; Zhi, M.; Frenking, G. The strength of a chemical bond. International Journal of Quantum Chemistry **2022**, 122, 26773 (9).

(48) Dassenoy, F.; Philippot, K.; Ely, T. O.; Amiens, C.; Lecante, P.; Snoeck, E.; Mosset, A.; Casanove, M.-J.; Chaudret, B. Platinum nanoparticles stabilized by CO and octanethiol ligands or polymers : FT-IR, NMR, HREM and WAXS studies. New Journal of Chemistry **1998**, 703–721.

(49) Gan, L.; Yu, R.; Luo, J.; Cheng, Z.; Zhu, J. Lattice strain distributions in individual dealloyed Pt–Fe catalyst nanoparticles. The journal of physical chemistry letters **2012**, 3, 934–938.

(50) Nilsson Pingel, T.; Jørgensen, M.; Yankovich, A. B.; Grönbeck, H.; Olsson, E. Influence of atomic site-specific strain on catalytic activity of supported nanoparticles. Nature communications **2018**, 9, 1–9.

(51) Hugenschmidt, M.; Adrion, K.; Marx, A.; Müller, E.; Gerthsen, D. Electron-Beam-Induced Carbon Contamination in STEM-in-SEM: Quantification and Mitigation. Microscopy and Microanalysis **2022**, ozac003.

(52) Demuth, J. E.; Jepsen, D. .; Marcus, P. M. Crystallographic Dependence of Chemisorption Bonding for Sulfur on Sulfur on (001), (110) and (111) Nickel. Physical Review Letters **1974**, 32, 1182–1185.

(53) Harrison, M. J.; Woodruff, D. P.; Robinson, J.; Sander, D.; Pan, W.; Kirschner, J. Adsorbate-induced surface reconstruction and surface-stress changes in Cu (100) O: Experiment and theory. Physical Review B **2006**, 74, 165402(7).

(54) Hitosugi, T.; Heike, S.; Onogi, T.; Hashizume, T.; Watanabe, S.; Li, Z.-Q.; Ohno, K.; Kawazoe, Y.; Hasegawa, T.; Kitazawa, K. Jahn-Teller Distortion in Dangling-Bond Linear Chains Fabricated on a Hydrogen-Terminated Si(100)-2 3 1 Surface. Physical Review Letters **1999**, 82, 4034–4037.

(55) Ibach, H. The role of surface stress in reconstruction, epitaxial growth and stabilization of mesoscopic structures. Surface Science Reports **1997**, 29, 195–263.

(56) Leyssens, T.; Peeters, D.; Orpen, A. G.; Harvey, J. N. How important is metal - Ligand back-bonding toward YX3 ligands (Y = N, P, C, Si)? An NBO analysis. Organometallics **2007**, 26, 2637–2645.

(57) Marzun, G.; Streich, C.; Jendrzej, S.; Barcikowski, S.; Wagener, P. Adsorption of Colloidal Platinum Nanoparticles to Supports: Charge Transfer and Effects of Electrostatic and Steric Interactions. Langmuir **2014**, 30, 11928–11936.

(58) Koczkur, K. M.; Mourdikoudis, S.; Polavarapu, L.; Skrabalak, S. E. Polyvinylpyrrolidone (PVP) in nanoparticle synthesis. Dalton Transactions **2015**, 44, 17883–17905.

(59) García-Aguilar, J.; Navlani-García, M.; Ángel Berenguer-Murcia,; Mori, K.; Kuwahara, Y.; Yamashita, H.; Cazorla-Amorós, D. Evolution of the PVP-Pd surface interaction in nanoparticles through the case study of formic acid decomposition. Langmuir **2016**, 32, 12110–12118.

TOC Graphic